N O T I C E

THIS DOCUMENT HAS BEEN REPRODUCED FROM MICROFICHE. ALTHOUGH IT IS RECOGNIZED THAT CERTAIN PORTIONS ARE ILLEGIBLE, IT IS BEING RELEASED IN THE INTEREST OF MAKING AVAILABLE AS MUCH INFORMATION AS POSSIBLE

JPL PUBLICATION 81-63

Scattering of Pruppacher-Pitter Raindrops at 30 GHz

C. Yeh
University of California, Los Angeles

R. Woo
Jet Propulsion Laboratory

A. Ishimaru
University of Washington

J. W. Armstrong
Jet Propulsion Laboratory

August 1, 1981

National Aeronautics and
Space Administration

Jet Propulsion Laboratory
California Institute of Technology
Pasadena, California

JPL PUBLICATION 81-63

Scattering of Pruppacher-Pitter Raindrops at 30 GHz

C. Yeh
University of California, Los Angeles

R. Woo
Jet Propulsion Laboratory

A. Ishimaru
University of Washington

J. W. Armstrong
Jet Propulsion Laboratory

August 1, 1981

National Aeronautics and
Space Administration

Jet Propulsion Laboratory
California Institute of Technology
Pasadena, California

The research described in this publication was carried out by the Jet Propulsion Laboratory, California Institute of Technology, under contract with the National Aeronautics and Space Administration.

Abstract

Optimum design of modern ground-satellite communication systems requires the knowledge of rain-induced differential attenuation, differential phase shift, and cross-polarization factors. After a rather comprehensive assessment of different available analytical techniques, an efficient technique is chosen to yield the desired scattering results. Tabulation of the scattered fields for Pruppacher-Pitter raindrops with sizes ranging from 0.25 mm to 3.5 mm at 20^{o} C and at 30 GHz for several incidence angles is given.

TABLE OF CONTENTS

I. Introduction.

The optimum design of modern ground-satellite communication systems requires detailed knowledge of the rain-induced radio propagation effects.[1-5] Investigation by Pruppacher and Pitter[6] on the shapes of realistic raindrops shows that raindrops take on shapes which deviate significantly from spheres when their sizes exceed about 1 mm. In fact their shapes even depart noticeably from oblate spheroidal shapes. It is well known according to the electromagnetic scattering theory that the shape of a scatterer is a crucial factor in determining the resonant scattering characteristics of a particle. Hence, accurate treatment of the scattering of realistic non-spherical shape raindrops is essential in the determination of rain-induced radio propagation effects which may include the generation of cross polarized fields[1] and the introduction of incoherent fields due to the presence of multiple scattering phenomenon.[8]

Various aspects of the rain scattering problems have been treated by a number of investigators using various justifiable or sometimes marginal techniques.[2-5] The purpose of this paper is twofold. We shall first provide a rather comprehensive assessment of previously used techniques. Based on our assessment we shall then select the most attractive method for rain-scattering calculation. Then, complete tabulation of scattered fields for Pruppacher-Pitter varying-shape raindrops with sizes ranging from 0.25 mm to 3.5 mm at 20° C and at 30 GHz for several incidence angles will be given. These extensive single particle scattering results also represent the necessary input for the determination of the distribution of incoherent and coherent intensities due to multiple scattering effects.[8]

II. An Assessment of Available Techniques for the Raindrop Scattering Problems.

The classical solutions of electromagnetic wave scattering are limited to simple objects of separable boundaries such as spheres, cylinders, etc. Recent developments in scattering analysis for scatterers of arbitrary shapes include the geometric theory of diffraction for high frequency scattering [9] and the method of moment,[10] the perturbation method,[11] the point matching method,[5] the extended boundary conditions method,[7] and the finite element technique for resonant region scattering.[12]

To achieve a proper perspective of the state-of-the-art of various analytical/numerical techniques, an assessment is made in the following:

(a) Geometrical Theory of Diffraction.

This method is mainly a high frequency technique which treats the smooth part of the scatterer by geometric optics and obtains the scattered fields from edges and glazing surfaces via solutions of canonical problems such as scattering by wedges, tips, etc. The geometric theory of diffraction may yield reasonable results even at resonant frequencies. However, it is still a technique most conveniently applied to convex and perfectly conducting targets at high frequencies. When the targets are concave or transparent, tracing the multiple scattering rays makes the method overly cumbersome to use.

Advantages:

Easy to learn

Clear physical concept

Disadvantages:

Difficult to apply to dielectric bodies.

Questionable validity at lower frequencies.

(b) Method of Moment

This method is based on the solution of an integral equation. The equation is a surface integral equation if the scatterer is a perfectly conducting body, a pair of coupled surface integral equation if the scatterer is a homogeneous dielectric body, and a volume integral equation if the scatterer is an inhomogeneous dielectric body. If the dielectric scatterer has a volume greater than $(0.1\lambda)^3$, the demand of the method of moment for computer memory or time becomes excessive.

Advantages:

Efficient for thin conducting scatterer.

Disadvantages:

Limited to dielectric scatterer of small volume.

(c) Perturbation Method.

This method is an extension of the Mie scattering solution to scatterers of non-spherical geometry by the boundary perturbation technique. This technique is inherently limited to particle shapes which are small perturbations of a sphere.

Advantages:

Analytic expressions are available.

Disadvantages:

Uncertain convergence

Limited to bodies that are small perturbations of a sphere.

Analytic expressions for higher-order terms are excessively complicated.

(d) Point Matching Method

Field expressions for the interior region of the scatterer and for the

exterior region are given in terms of complete sets of spherical harmonics. Boundary conditions are satisfied by point-matching on the boundary surface.

Advantages:

Conceptually simple

Disadvantages:

Uncertain convergence

Demands excessive computer time

Limited to bodies that are close to spherical shapes

(e) Extended Boundary Condition Method.

Integral representations for the fields can be derived which satisfy the wave equation and all necessary boundary conditions. By expanding the fields in terms of a complete set of spherical harmonics and by making use of analytic continuation techniques, one may reduce the integral representations to a set of linear algebraic equations.

Advantages:

May be used to treat scatterers of large volume and arbitrary shapes

Numerical results can be generated very efficiently

Disadvantages:

Usually not applicable to inhomogeneous dielectric scatterers

(f) Global-Local Finite Element Method.

The term Global-Local Finite Element Method refers to a numerical analysis technique in which both the contemporary finite element and classical Rayleigh-Ritz approximations are employed. The scattering problem is divided into two regions: the exterior region and the interior region. Without any sacrifice

of rigor, it is assumed that the boundary surface between the exterior and interior regions is a sphere for three-dimensional problems and a circular cylinder for two-dimensional problems. It is further assumed that the boundary surface is so chosen that the medium in the exterior region is homogeneous and that the inhomogeneous irregularly-shaped absorbing object is contained within the interior region. Solutions of wave equations in the exterior homogeneous region are well-known. Therefore, knowing the interior fields at the boundary surface provides the necessary information to solve the exterior fields by using the boundary conditions at the boundary surface. The finite-elements technique is used to find the interior field.

Advantages:

Adaptable to scatterers of non spherical shapes and inhomogeneous material.

Results are based on exact Maxwell's equations.

Disadvantages:

Requires extensive computer memory.

Complicated computer codes.

Based on this assessment it is noted that only two techniques are sufficiently reliable to provide scattering results that possess little uncertainty for Pruppacher and Pitter raindrops. They are the extended boundary condition method and the finite element technique. The complexity of the finite element formulation for truly three dimensional problems and its enormous demand for computer memory renders this technique less than attractive for extensive computations. The extended boundary condition technique is therefore preferred.

III. A Brief Summary of the Extended Boundary Condition Method.

The geometry of the problem is shown in Fig. 1. For a linearly polarized incident plane wave

$$\underline{E}_i(z) = E_o e^{jkz} \underline{e}_i \tag{1}$$

where E_o is the amplitude of the plane wave, $\underline{e}_i$ is a unit vector indicating the polarization direction of the incident wave which is taken to be either the x or y direction, k is the free-space wave number, and the wave is propagating in the +z direction, the scattered field takes on the following form:

$$\underline{E}_s(r) = \underline{f}\ (\underline{o}, \underline{i})\ \frac{e^{ikR}}{R} \tag{2}$$

where $\underline{i}$ and $\underline{o}$ are, respectively, the incident direction and the observation direction. Following the matrix notation of Ishimaru [1978] and Van de Hulst [1957], the incident field and the far-zone scattered field can be written as follows:

$$\begin{aligned} \underline{E}_i &= E_{i\perp}\, \underline{e}_{i\perp} + E_{i//}\, \underline{e}_{i//} \\ \underline{E}_s &= E_{s\perp}\, \underline{e}_{s\perp} + E_{s//}\, \underline{e}_{s//} \end{aligned} \tag{3}$$

where $\underline{e}_{i\perp}$ or $\underline{e}_{s\perp}$ and $\underline{e}_{i//}$ or $\underline{e}_{s//}$ are, respectively the unit vectors perpendicular and parallel to the plane of scattering which is the plane containing the vectors $\underline{i}$ and $\underline{o}$. Note that $\underline{e}_i$ is necessarily equal to $\underline{e}_s$, but $\underline{e}_{i//}$ is not necessarily equal to $\underline{e}_{s//}$ and $E_{s\perp}$ and $E_{s//}$ are related to $E_{i\perp}$ and $E_{i//}$ by the following relation:

$$\begin{bmatrix} E_{s\perp} \\ E_{s//} \end{bmatrix} = \frac{e^{ikR}}{R} \begin{bmatrix} f_{11} & f_{12} \\ f_{21} & f_{22} \end{bmatrix} \begin{bmatrix} E_{i\perp} \\ E_{i//} \end{bmatrix} \tag{4}$$

The scattering functions S_1, S_2, S_3 and S_4 used by Van de Hulst as well as the Stokes parameters can all be obtained from f_{11}, f_{12}, f_{21} and f_{22}. For example:

$$S_1 = \frac{k}{i} f_{11},\ S_2 = \frac{k}{i} f_{22},\ S_3 = \frac{k}{i} f_{21},\ S_4 = \frac{k}{i} f_{12} \tag{5}$$

and if the incident wave has an arbitrary state of polarization and its Stokes parameters are given by I_{1i}, I_{2i}, U_i and V_i, then the Stokes parameters I_{1s}, I_{2s}, U_s, and V_s of the scattered wave are given by

$$\begin{bmatrix} I_{1s} \\ I_{2s} \\ U_s \\ V_s \end{bmatrix} = \frac{1}{R^2} \begin{bmatrix} |f_{11}|^2 & |f_{12}|^2 & \mathrm{Re}(f_{11}f_{12}^*) & -\mathrm{Im}(f_{11}f_{12}^*) \\ |f_{21}|^2 & |f_{22}|^2 & \mathrm{Re}(f_{21}f_{22}^*) & -\mathrm{Im}(f_{21}f_{22}) \\ 2\mathrm{Re}(f_{11}f_{21}) & 2\mathrm{Re}(f_{12}f_{22}^*) & \mathrm{Re}(f_{11}f_{22}^*+f_{12}f_{21}^*) & -\mathrm{Im}(f_{11}f_{22}^*+f_{12}f_{21}^*) \\ 2\mathrm{Im}(f_{11}f_{21}) & 2\mathrm{Im}(f_{12}f_{22}^*) & \mathrm{Im}(f_{11}f_{22}^*+f_{12}f_{21}^*) & \mathrm{Re}(f_{11}f_{22}^*+f_{12}f_{21}^*) \end{bmatrix} \begin{bmatrix} I_{1i} \\ I_{2i} \\ U_i \\ V_i \end{bmatrix} \tag{6}$$

where * means the complex conjugate.

Other commonly used parameters may also be defined in terms of the function $\underline{f}\ (\underline{o}, \underline{i})$; such as:

The differential scattering cross section, $\sigma_d(\underline{o}, \underline{i}) = |f\ (\underline{o}, \underline{i})|^2$ (7)

The bistatic radar cross section, $\sigma_{bi}\ (\underline{o}, \underline{i}) = 4\pi\ |f(\underline{o}, \underline{i})|^2$ (8)

The backscattering cross section, $\sigma_b = 4\pi\ |f(-\underline{i}, \underline{i})|^2$ (9)

The scattering cross section, $\sigma_s = \int_{4\pi} |f\ (\underline{o}, \underline{i})|^2\ d\Omega$ (10)

($d\Omega$ = differential solid angle)

The extinction cross section, $\sigma_\lambda = \sigma_s + \sigma_a$

$$= \frac{4\pi}{k} \mathrm{Im}\ (f(\underline{i},\underline{i}))\cdot\underline{e}_i = \frac{4\pi}{k} \mathrm{Im}(f_{11}(o)) = \frac{4\pi}{k} \mathrm{Im}(f_{22}(o)) \tag{11}$$

(σ_a = absorption cross section, $\underline{e}_i$ = unit vector in the direction of polarization of the incident wave.)

So, knowing the matrix elements f_{11}, f_{12}, f_{21}, f_{22}, one may calculate all the desired parameters. These matrix elements are obtained by solving the boundary value problem. We intend to use the extended boundary condition technique to solve this scattering problem.

The scattering body, assumed to be homogeneous and isotropic, is characterized by the constitutive parameters μ_o and ϵ where μ_o is the free space permeability and ϵ is the permittivity of the dielectric material (ϵ may be complex to account for the lossy case). The surrounding medium is considered to be free space with parameters μ_o, ϵ_o. For the given incident field, the scattered field must be determined.

The theoretical development for the extended boundary conditon technique is as follows:

First, the Equivalence Principle is applied, breaking the scattering problem into two separate problems, an exterior part and an interior part. One equation for the unknown field quantities is derived from the external problem where it is found that the scattered field due to the surface currents must completely cancel the incident field throughout the interior volume.

The internal problem is then considered and the fields within the dielectric region are expanded in regular vector spherical wave functions with coefficients to be determined. Superposition is applied and the boundary conditions at the surface lead to a linear system of integral equations for the coefficients of the unknown surface fields in terms of the incident field.

The scattered far field is then determined by evaluating the internal field at the surface and substituting into the original expression which gives the exterior scattered field in terms of the surface fields.

To avoid writing many lengthy mathematical expressions, detailed derivation will not be given here. We shall simply state the final results:

$$(K + \sqrt{\epsilon_r} J)\, c_\mu + (L + \sqrt{\epsilon}\, I)\, d_\mu = -j a_\nu \qquad (12)$$

$$\nu = 1,2,\ldots,N$$

$$(I + \sqrt{\epsilon_r} L)\, c_\mu + (J + \sqrt{\epsilon_r} K)\, d_\mu = -j b_\nu \qquad (13)$$

where

$$I = \frac{k^2}{\pi} \int_S \underline{n}.\underline{M}^3_\nu\,(k\underline{r}') \times \underline{M}^1_\mu\,(k'r')dS$$

$$J = \frac{k^2}{\pi} \int_S \underline{n}.\underline{M}^3_\nu\,(k\underline{r}') \times \underline{N}^1_\mu\,(k'\underline{r}')dS$$

$$K = \frac{k^2}{\pi} \int_S \underline{n}.\underline{N}^3_\nu\,(k\underline{r}') \times \underline{M}^1_\mu\,(k'\underline{r}')dS$$

$$L = \frac{k^2}{\pi} \int_S \underline{n}.\underline{N}^3_\nu\,(k\underline{r}') \times \underline{N}^1_\mu\,(k'\underline{r}')dS$$

and $\epsilon_r = \frac{\epsilon}{\epsilon_o}$. $\underline{n}$ is a unit vector normal to the boundary surface S and r' is the radial vector from the origin to the boundary surface. a_ν and b_ν are expansion coefficients for the incident wave defined as follows:

$$\underline{E}_i(r) = \sum_{\nu=1}^{\infty} D_\nu \left[a_\nu \underline{M}^1_\nu(kr) + b_\nu \underline{N}^1_\nu(k\underline{r})\right] \qquad (14)$$

where ν is a combined index incorporating σ, m and n. D_ν is a normalization constant

$$D_\nu = \epsilon_m \frac{(2n+1)(n-m)!}{4n(n+1)(n+m)!}\,, \quad \epsilon_m = \begin{cases} 1 \\ 2 \end{cases}, \quad \begin{matrix} m = 0 \\ m > 0 \end{matrix}$$

The spherical wave harmonics $\underline{M}$ and $\underline{N}$ have been defined by Stratton[10]. These functions, solutions of the vector wave equation, are given by,

$$\underline{M}^{1,3}_{\sigma mn}(\underline{r}) = \nabla \times \underline{r} \begin{matrix} \cos m\phi \\ \sin m\phi \end{matrix} P^m_n(\cos\theta) z^{1,3}_n(kr) \qquad (15)$$

$$\underline{N}^{1,3}_{\sigma mn}(\underline{r}) = \frac{1}{k} \nabla \times \underline{M}^{1,3}_{\sigma mn}(\underline{r})$$

where σ = even or odd,

$P_n^m(\cos\theta)$ = associated Legendre function,

and $z_m^{1,3}(kr)$ = an appropriate spherical Bessel function.

For solutions of the wave equation which must be finite at r = 0, $z_n^1(kr)$ = $j_n(kr)$ and the resulting vector spherical functions $\underline{M}$ and $\underline{N}$ are known as solutions of the first kind. The other vector spherical functions we will be using are obtained by using the spherical Hankel functions, i.e., $z_n^3(kr) = h_n^{(1)}(kr) = j_n(kr) + jn_n(kr)$. This solution, representing outgoing waves, is called the solution of the third kind.

c_μ and d_μ are the expansion coefficients for the field inside the dielectric which are defined as follows:

$$\underline{E}(k'\underline{r}) = \sum_{\mu=1}^{N} [c_\mu \underline{M}_\mu^1(k'\underline{r}) + d_\mu \underline{N}_\mu^1(k'\underline{r})] \tag{16}$$

where μ incorporates the indices σ, m, n and c_μ and d_μ are unknown coefficients. $k' = \sqrt{\epsilon_r}k$ and $k = \omega\sqrt{\mu_o\epsilon_o}$. The H field internal to S is given by

$$\underline{H}(k'\underline{r}) = \frac{1}{j\omega\mu_o}(\nabla \times \underline{E}(k'\underline{r}))$$

$$= \frac{1}{j\omega\mu_o}\sum_{\mu=1}^{N}[c_\mu(\nabla \times \underline{M}_\mu^1(k'\underline{r}) + d_\mu\ (\nabla \times \underline{N}_\mu^1(k'\underline{r}))]$$

$$= -j\frac{\epsilon}{\mu_o}\sum_{\mu=1}^{N}[c_\mu \underline{N}_\mu^1(k'\underline{r}) + d_\mu \underline{M}_\mu^1(k'\underline{r})] \tag{17}$$

The coefficients of the scattered fields which are defined as follows:

$$\underline{E}_s(k\underline{r}) = \sum_{\nu=1}^{N}[p_\nu \underline{M}_\nu^3(k\underline{r}) + q_\nu \underline{N}_\nu^3(k\underline{r})] \tag{18}$$

where r is outside a circumscribed sphere, are

$$p_\nu = -jD_\nu \sum_{\mu=1}^{N} \{[K' + \sqrt{\epsilon_r} J'] c_\mu + [L' + \sqrt{\epsilon_r} I'] d_\mu\}$$

$$q_\nu = -jD_\nu \sum_{\mu=1}^{N} \{[I' + \sqrt{\epsilon_r} L'] c_\mu + [J' + \sqrt{\epsilon_r} K'] d_\mu\} \qquad (19)$$

where

$$I' = \frac{k^2}{\pi} \int_s \underline{n} . \underline{M}_\nu^1(k\underline{r}') \times \underline{M}_\mu^1(k'\underline{r}') dS$$

$$J' = \frac{k^2}{\pi} \int_s \underline{n} . \underline{M}_\nu^1(k\underline{r}') \times \underline{N}_\mu^1(k'\underline{r}') dS$$

$$K' = \frac{k^2}{\pi} \int_s \underline{n} . \underline{N}_\nu^1(k\underline{r}') \times \underline{M}_\mu^1(k'\underline{r}') dS$$

$$L' = \frac{k^2}{\pi} \int_s \underline{n} . \underline{N}_\nu^1(k\underline{r}') \times \underline{N}_\mu^1(k'\underline{r}') dS.$$

The exact theoretical problem requires the solution of an infinite set of equations. The equations resulting from the External Problem are such a set. The first concession to practical considerations is made in the derivation of the Internal Problem, where the infinite term spherical expansion for the internal field is truncated to N terms. This finite internal field expansion is then substituted into the first 2N equations of the infinite set of Eqs. (13) and the final set of truncated equations is obtained. The scattering results are obtained numerically by solving the complete set of equations for successive values of N until the final results (such as the differential scattering cross section) converge to a specified accuracy. This insures that enough of the expansion terms have been kept to guarantee the correct final result.

The indices μ and ν each run from 1 to N and are related to the internal field expansions respectively. As indicated previously, they incorporate the indices σ, m and n where σ is even or odd and m and n are indices of Bessel and Legendre functions. To distinguish between expansions over ν and μ, the indices which they represent are unprimed and primed, respectively, i.e.,

ν is over σ, m, n

μ is over σ', m', n'

where the expansion scheme is as follows:

σmn = e01, o01, e11, o11, e02, o02, e12, o12, e22, o22, ...

where e = even and o = odd.

There are essentially four main steps in the solution for the differential scattering cross section.

(1) Solution of the system of Eqs. (13) for the coefficients of the internal field c_μ and d_μ in terms of the incident field coefficients a_μ and b_μ and S is the surface of the scattering object. Note that the solution of the Eqs. (13) requires a matrix inversion procedure.

(2) Substitution of the coefficients c_μ and d_μ into Eqs. (19) to determine the coefficients of the scattered field.

(3) Substitution of the scattered field coefficients into a spherical expansion for the far field vector amplitude.

$$f(\theta_s,\phi_s|\theta_i,\phi_i) = \frac{1}{jk} \sum_{\nu=1}^{N} [p_{\nu} \underline{C}_{\nu}(\theta,\phi) + jq_{\nu} \underline{B}_{\nu}(\theta,\phi)$$

(4) Computation of the differential scattering cross section

$$\sigma_d(\theta_s,\phi_s) = |f(\theta_s,\phi_s|\theta_i,\phi_i)|^2$$

IV. Display of Results and Discussion

Selected Pruppacher-Pitter raindrop shapes are displayed in Fig. 2. It can be seen that as the raindrop size increases, its shape deviates significantly from a sphere and it even differs noticeably from an oblate spheroid. These Pruppacher-Pitter raindrop shapes were used in our computation and compilation of the scattering results. Specifically, we have obtained the scattering matrix elements f_{11}, f_{12}, f_{21}, f_{22} for the following parameters:

Raindrop sizes: 0.25 mm (0.25 mm) 3.5 mm

Frequency: 30 GHz

Temperature: 20°C

θ_s: 0° (10°) 360°

α : 0° (30°) 90°

ϕ_s: 0° (30°) 180°

Results are tabulated in Table 1 which has been condensed into the two microfiches attached at the end of this report.

We have, of course, compared our results with those obtained by Cross and Morrison[4], and Oguchi[5] who used the point-matching technique and by Morgan[12] who used the finite-element approach. The results all agree within a few percentage points. These differences may be caused by numerical errors due to finite grid size, finite number of matching points, finite matrix size, finite integration steps, accumulated numerical errors or the limitation of the particular numerical scheme. Based on this comparison, one may conclude that the point-matching technique actually provides rather good results in spite of uncertain convergence and the lack of rigor due to "Rayleigh Phenomenon." It is also significant to note that our results agree

quite well with those obtained according to the finite-element approach which is based on the exact Maxwell equations.

It is of interest to note that the scattering results for a Pruppacher-Pitter shaped raindrop compared very closely to those for an equivalent oblate spheroidal shaped raindrop even when their shapes are visibly different for large size drops (see Fig. 2). It appears that the absorptive characteristics of water at 30 GHz and 20° C are responsible for minimizing the differences in the scattering results due to shape differences in the Pruppacher-Pitter and equivalent oblate spheroidal drops.

To illustrate the effect of drop size changes on the scattered field, Figs. 3-5 are introduced. In Fig. 3 the normalized scattering, absorption and extinction cross-sections are plotted as a function of raindrop sizes. The relatively smooth character of the curves can again be attributed to the absorptive nature of water. Polar plots of scattered fields in the $\phi_s = 90^\circ$ plane for canting angles $\alpha = 0^\circ$ and 60° and for various drop sizes are shown in Figs. 4-6. It can be seen that no cross polarized field is generated for small drop sizes (with spherical shapes) or for canting angle $\alpha = 0$. (See Fig. 4.) For large drop sizes (with non spherical shapes) and for canting angle $\alpha \neq 0$, a cross polarized field is generated. (See Fig. 5 and 6.) One also notes that the induced cross polarized field is at least one order of magnitude weaker than the non-cross polarized scattered field. This is again due to the absorptive characteristics of the raindrops under consideration.

In conclusion one may state that the extended boundary condition method is an efficient method in yielding reliable scattering results for non-spherical Pruppacher-Pitter raindrops. One notes that the large absorption

constant of water at 30 GHz and 20° C tends to minimize the shape effect on the scattered field. It is expected that, due to the transparent nature of ice at 30 GHz, the shape factor for ice particles will play a significant role in giving rise to the generation of cross polarized field.

Acknowledgment

The authors wish to thank Prof. H. R. Pruppacher of UCLA for his advice on raindrop shapes and his interest in this work.

REFERENCES

1. M.J. Saunders, IEEE Trans. on Ant. and Prop. AP-19, 273 (1971).
2. T.S. Chu, Bell Sys. Tech. J. 53, 1557 (1974).
3. D.J. Fang, COMSAT Tech. Rev. 6, 29 (1976).
4. J.A. Morrison and M.J. Cross, Bell Sys. Tech. J. 53, 955 (1974).
5. T. Oguchi, Radio Science 12, 41 (1977).
6. H.R. Pruppacher and R.L.Pitter, J. Atmos. Sci. 28, 86 (1971).
7. P. Barber and C. Yeh, Appl. Opt. 14, 2864 (1975).
8. A. Ishimaru,"Wave Propagation and Scattering in Random Media," Vol. I and II, Academic Press, New York (1978).
9. J.B. Keller, J. Opt. Soc. Am. 52, 116 (1962).
10. R.F. Harrington, "Field Computation by Moment Method" New York, MacMillan (1968).
11. C. Yeh, Phys. Rev. 135, A1193 (1964).
12. K.K. Mei, IEEE Trans. Ant. & Prop. AP-22, 760 (1974); C. Yeh, S.B. Dong and W. Oliver, J. Appl. Phys. 46, 2125 (1975); M.A. Morgan, Radio Science 15, 1109 (1981).

α = CANTING ANGLE

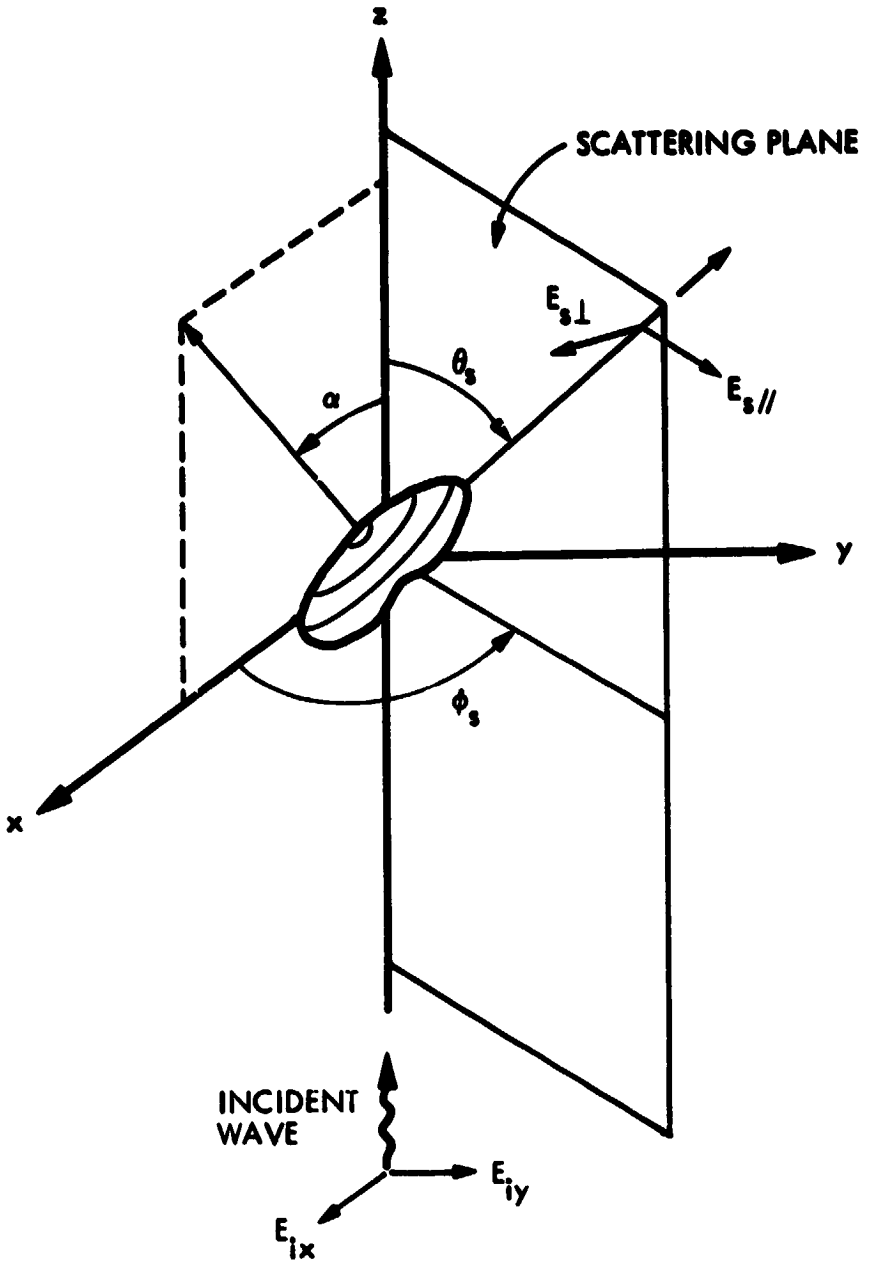

$$\begin{bmatrix} E_{s\perp} \\ E_{s//} \end{bmatrix} = \frac{e^{ikR}}{R} \begin{bmatrix} f_{11} & f_{12} \\ f_{21} & f_{22} \end{bmatrix} \begin{bmatrix} E_{iy} \\ E_{ix} \end{bmatrix}$$

Figure 1. The geometry of the problem.

PARAMETERS FOR CALCULATIONS

PRUPPACHER - PITTER RAINDROP SIZES 0.25 mm (0.25 mm) 3.5 mm

FREQUENCY: 30 GHz

TEMPERATURE: 20°C

$\alpha = 0^{\circ} (30^{\circ}) 90^{\circ}$

$\phi_s = 0^{\circ} (30^{\circ}) 180^{\circ}$

$\theta_s = 0^{\circ} (10^{\circ}) 360^{\circ}$

0.25 mm 1.5 mm 3.5 mm

RAINDROP SHAPES

Figure 2. Pruppacher-Pitter raindrops

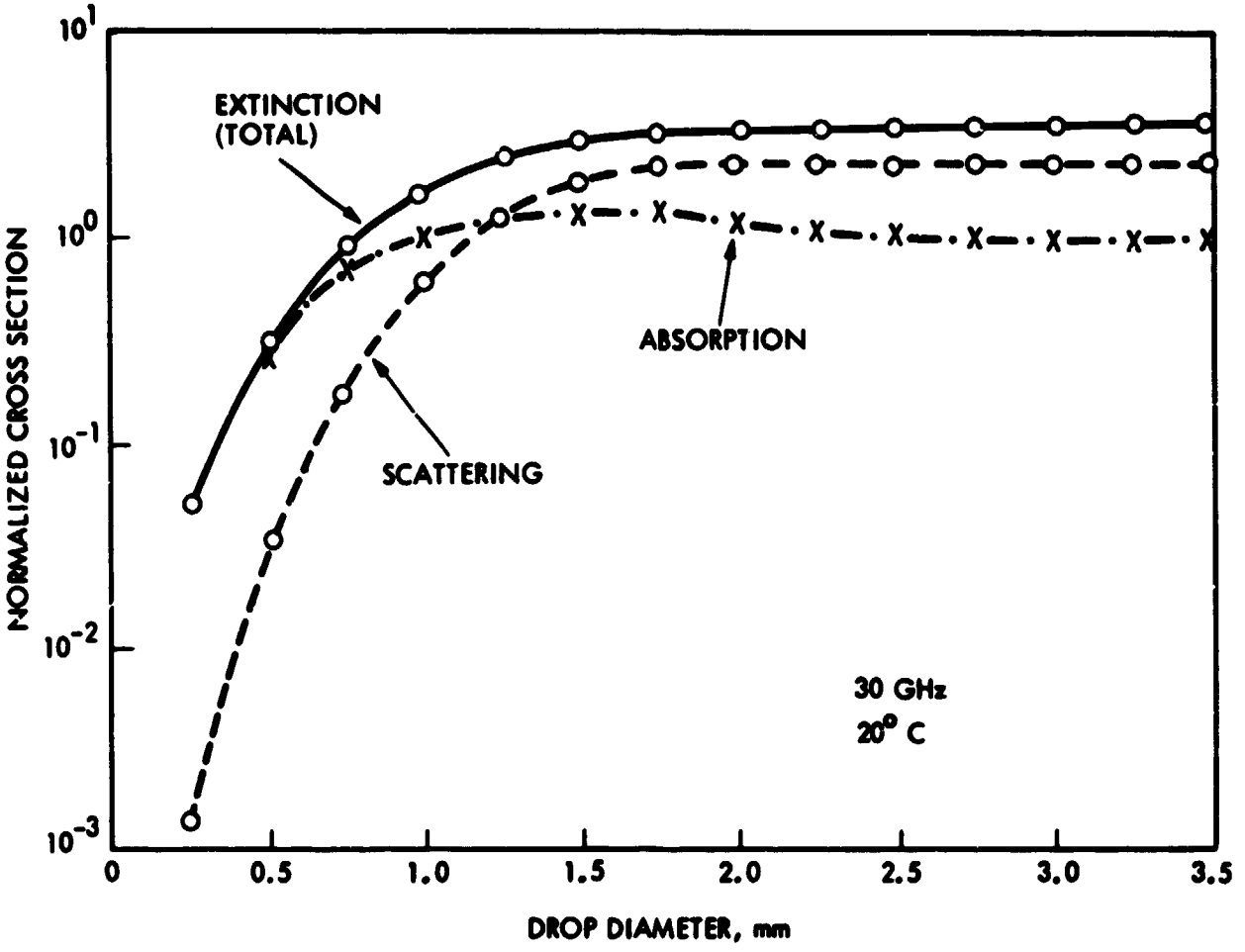

Figure 3. Normalized cross section as a function of raindrop size

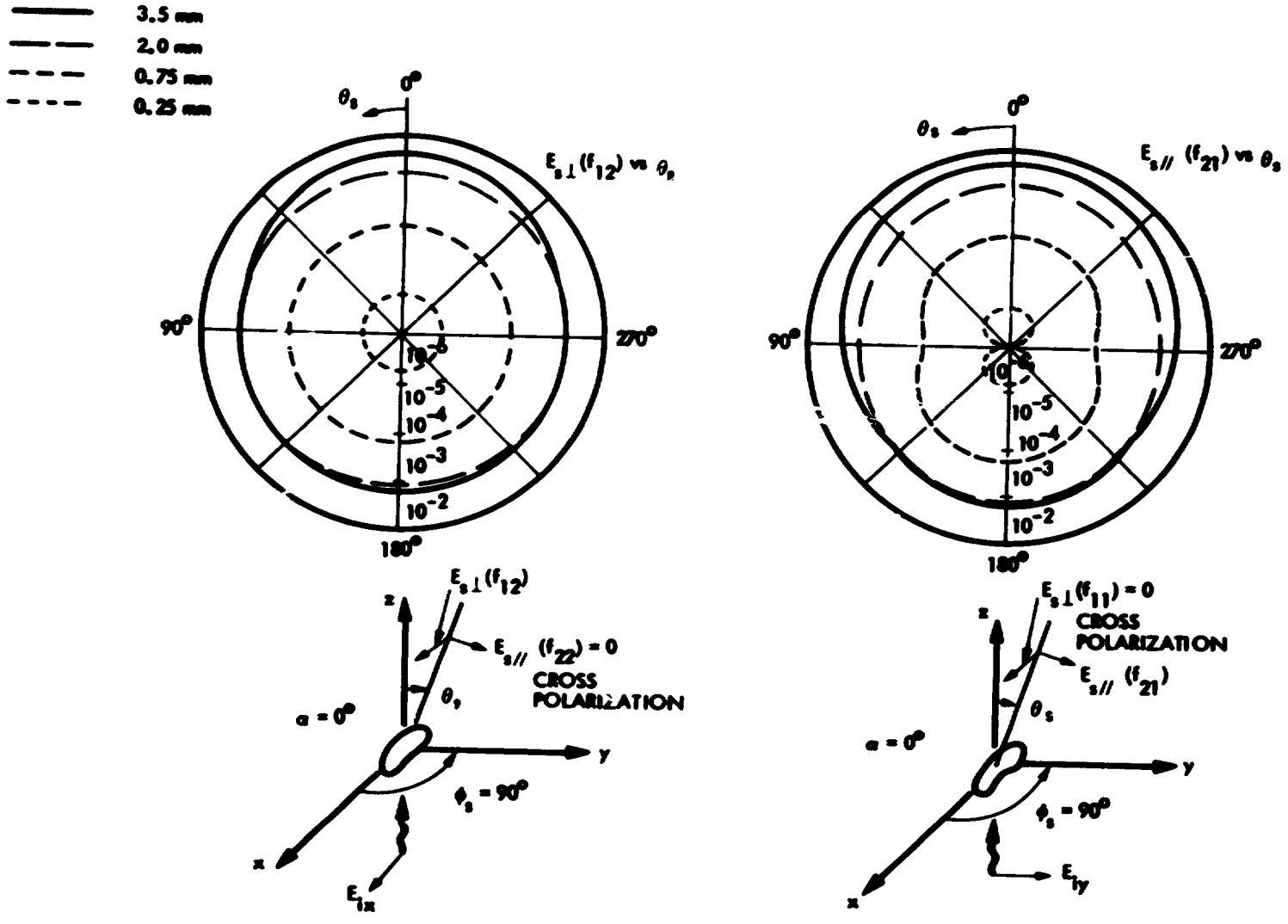

Figure 4. Polar diagrams for scattered fields with $\alpha = 0^{\circ}$ (no cross polarization)

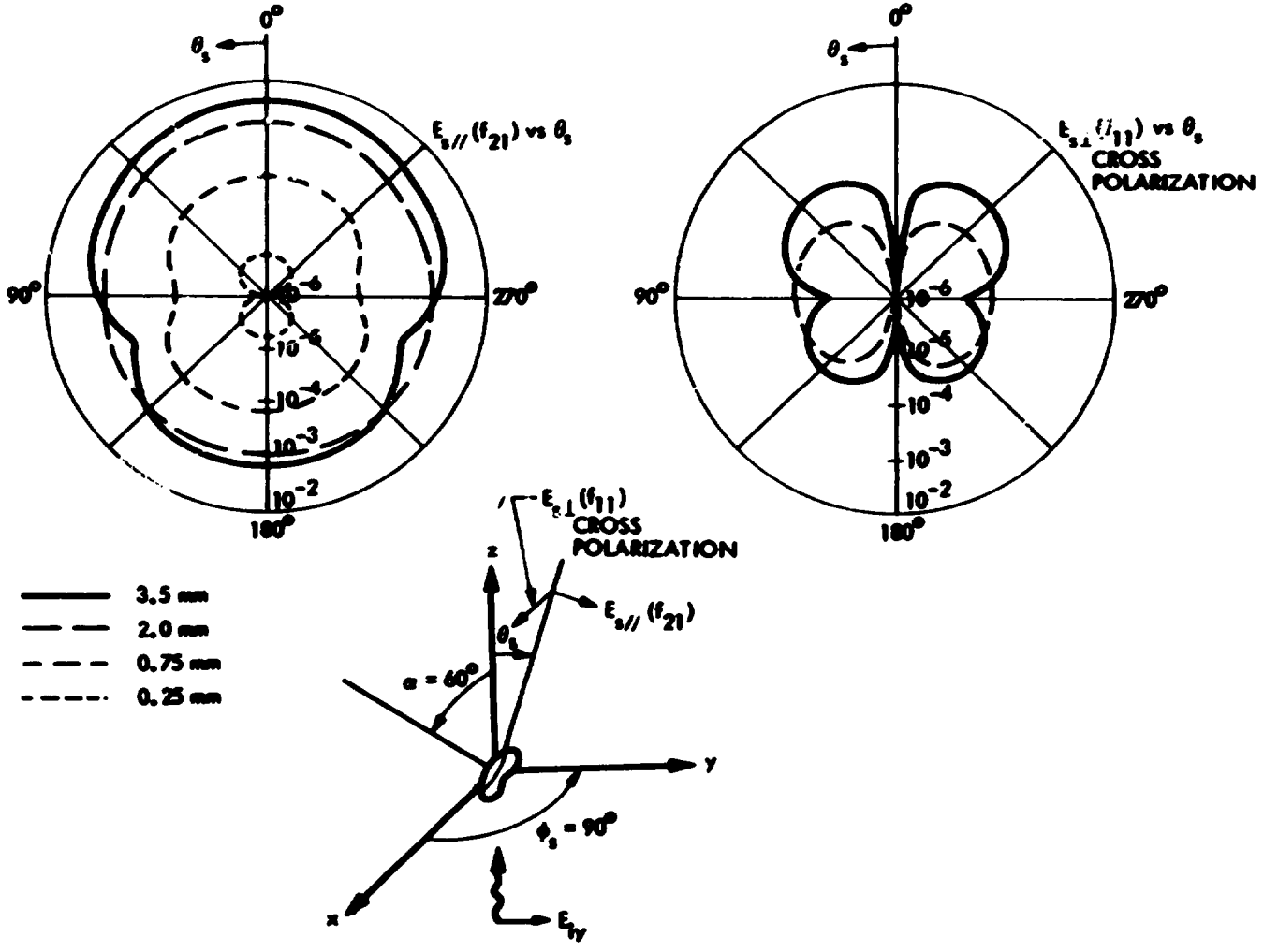

Figure 5. Polar diagrams for scattered fields with $\alpha = 60°$ (cross polarization present for non-spherical raindrops). Incident field is polarized in the y-direction.

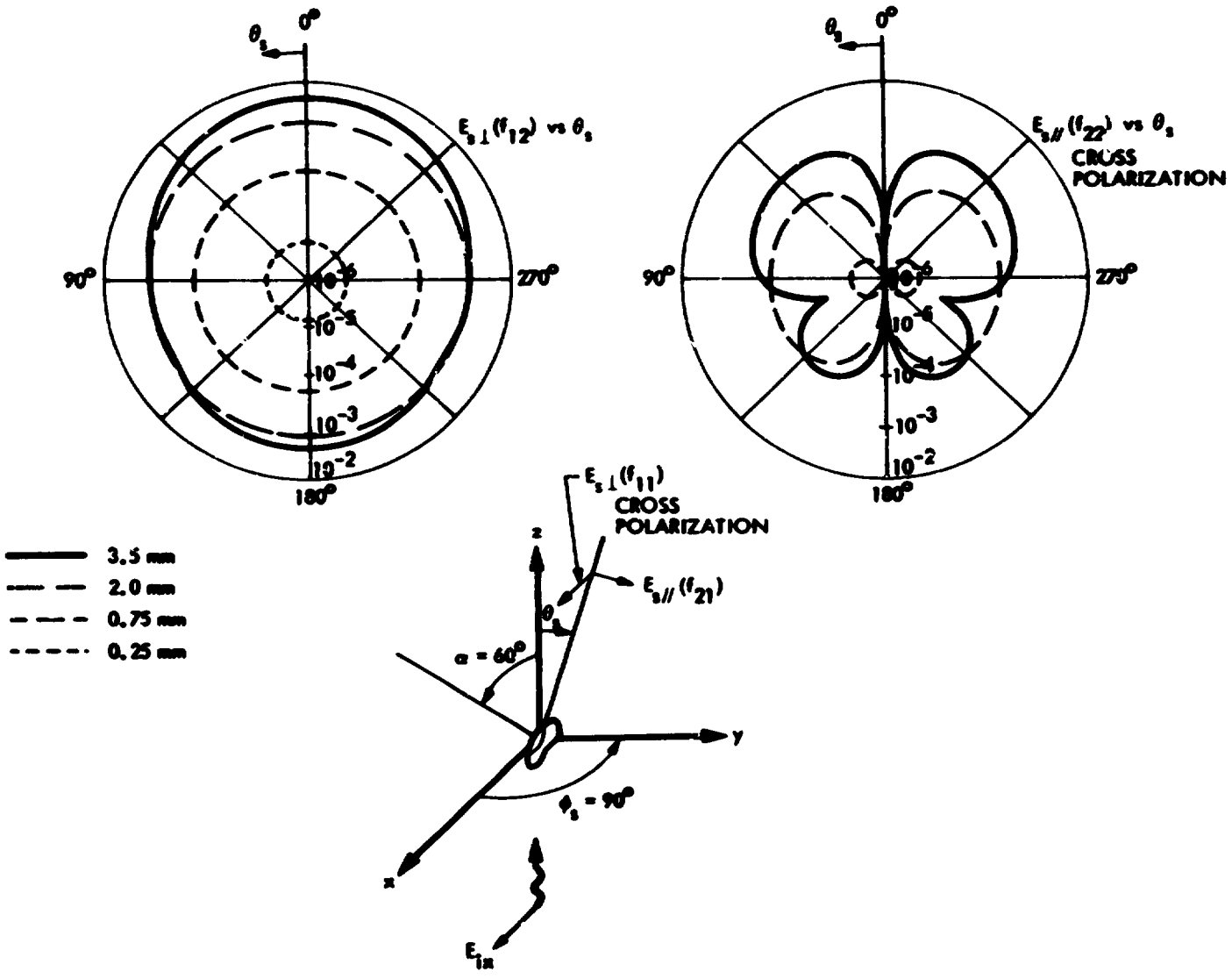

Figure 6. Polar diagrams for scattered fields with $\alpha = 60°$ (cross polarization present for non-spherical raindrops). Incident field is polarized in the x-direction.